Ab Initio Study on Spectroscopic Properties of GdF_3 and $GdCl_3$

Giuseppe Lanza* and Camilla Minichino

Dipartimento di Chimica, Università della Basilicata, via Nazario Sauro 85, 85100 Potenza, Italy

Received: January 19, 2004; In Final Form: March 25, 2004

The geometry and vibrational frequencies of the GdX_3 (X = F and Cl) molecules have been analyzed at the ab initio level with extended basis sets, employing relativistic effective core potential, and evaluating electronic correlation by means of second-order perturbative (MP2) and coupled cluster (CCSD and CCSD(T)) methods. Anharmonicities, temperature, and inert-gas matrix effects have been explicitly included. The MP2, CCSD, and CCSD(T) calculations on the systems in the gas phase indicate a trigonal planar equilibrium structure for $GdCl_3$ and a quasiplanar geometry for GdF_3. Vibrationally averaged bond angle, evaluated by means of a simple one-dimensional treatment, is considerably smaller than the equilibrium value and both molecules have a pyramidal thermal average structure, in agreement with recent electron diffraction measurements. The theoretical estimate of Gd−X bond lengths depends on both the electronic correlation treatment and the basis set quality, thus indicating the desirability of high-level calculations. Experimental and theoretical comparison becomes quantitative after including thermal correction. Anharmonic vibrational frequencies have been computed through the vibrational self-consistent field method followed by the second-order perturbation correction. For both gadolinium trihalides, the ν_2 out-of-plane bending potential shows a huge "negative" anharmonic form and hot bands fall at considerably higher energies than the fundamental one. Although the anharmonicities for the remaining modes are small, they are important for a correct interpretation of experimental IR spectra. The inert-gas matrix interactions, modeled by coordination of one and two inert-gas molecules $GdX_3 \cdot IG_m$ (IG = Ne, Ar, Xe, and N_2; m = 1 and 2), are substantial and GdX_3 structures strongly depend on the number of coordinating molecules and on the interaction strength. As a consequence, all normal-mode frequencies slightly diminish as GdX_3- -IG_m interactions grow, while the ν_2 out-of-plane bending frequency significantly increases.

Introduction

There is a great interest in the study of the molecular properties of monomeric lanthanide trihalides because of their importance in many fundamental aspects in structural,[1,2] spectroscopy,[3−7] and reactivity[8] and applicative fields of chemistry and physics.[9−13] As a consequence, a large quantity of experimental and theoretical research activity has been undertaken with the aim of elucidating their molecular properties.

Even though electron diffraction (ED) and vibrational spectroscopy characterizations of lanthanide trihalides have been reported over several decades, the matter is still the object of great debate and seems not to have been definitively assessed due to intrinsic problems raised by the high temperature (>1000 K) required for vaporization.[1,14,15] For example, high-temperature gas-phase IR experiments of free species suffer from peak broadening due to the population of many vibrational and rotational excited levels.[3,4] On the other hand, cryogenic temperature experiments with molecules trapped in solid inert-gas matrices are complicated by ion−induced-dipole interactions between molecules and the host matrix that cause vibrational frequency shifts and, in some cases, changes in molecular symmetry.[5−7] Hence two important pieces of information, such as vibrational frequencies and molecular symmetry, are not unequivocally determined. Recent technical refinements of ED experiments and new models for data analysis suggest that the thermal average structure (Ln−X and X- - -X distances) differs significantly from the equilibrium geometry.[1,14,15a] Often the symmetry of the thermal average structure is lower than that of the equilibrium arrangement because of soft angle deformation.

In this regard, electronic structure studies have been of great relevance to the experimental community in providing complementary and independent information on both the geometry and vibrational frequencies of lanthanide trihalides.[16−23] Nevertheless, such data, derived from the minimum of the potential energy surface of free species, are scarcely representative of the "true" molecular status in experiments, i.e., the comparison between experimental and computed spectroscopic parameters is not straightforward. In a preliminary communication, we clarified the significant effects of temperature, anharmonicity, and inert-gas matrix on spectroscopic properties.[24] The results argue that any reasonable experimental/theoretical data comparison must go beyond the standard quantum chemical calculations.

In the present contribution, we report a full account of our theoretical analysis at the ab initio MP2, CCSD, and CCSD(T) levels of two representative GdF_3 and $GdCl_3$ cases of lanthanide trihalides. We have explored in detail (i) equilibrium structures and harmonic vibrational frequencies of the molecules as a function of the size of the basis set and of the method employed in evaluating electronic correlation, (ii) thermal average structures emphasizing dynamic effects on the Gd−X bond length and X−Gd−X bond angle, (iii) anharmonic vibrational frequencies of fundamentals and hot bands to better rationalize gas-phase experimental IR spectra, and (iv) equilibrium structures and harmonic vibrational frequencies of model complexes $GdX_3 \cdot IG_m$ (IG = Ne, Ar, Xe, and N_2; m = 1 and 2) simulating

10.1021/jp049734e CCC: $27.50
Published on Web 05/12/2004

TABLE 1: Basis Sets Adopted in Calculations of GdX_3 Molecular Properties

		basis set contraction	
		gadolinium	halogen
TZ2D		[3111,3111,21,61]	[62111,411,11] [631111,52111,11]
TZ2DG	g polarization function on gadolinium ($\alpha = 0.4$)	[3111,3111,21,61,1]	[62111,411,11] [631111,52111,11]
TZ2DG+	sp diffuse function on halogens (F: $\alpha = 0.1076$; Cl: $\alpha = 0.0483$)	[3111,3111,21,61,1]	[621111,4111,11] [6311111,521111,11]
TZ2D2G+	g polarization function on gadolinium ($\alpha = 0.2$)	[3111,3111,21,61,11]	[621111,4111,11] [6311111,521111,11]
TZ2D2GF+	f function on gadolinium ($\alpha = 0.2$)	[3111,3111,21,611,11]	[621111,4111,11] [6311111,521111,11]
TZ2D2G2F+	f polarization function on halogens (F: $\alpha = 1.85$; Cl: $\alpha = 0.7$)	[3111,3111,21,611,11]	[621111,4111,11,1] [6311111,521111,11,1]
EXTENDED	small-core pseudopotentials and extended basis sets on gadolinium	[5111111111,61111111,61111,5111,411]	[621111,4111,11,1] [6311111,521111,11,1]

the host−guest interactions between GdX_3 molecules and inert-gas matrices with the aim of interpreting, at least qualitatively, spectroscopic IR data of real systems.

Computational Details

Electronic Structure Calculations. The relativistic effective core potentials (RECP) of Stevens et al.,[25] which explicitly treat semicore 5s and 5p and valence 4f electrons and a basis set contracted as [3111,3111,21,61], were used for the gadolinium atom. RECP for the xenon atom was also adopted to describe core electrons with a basis set contracted as [41,41].[25b] An extra "sp" function ($\alpha = 0.06$) was added to warrant compatibility and comparability of results obtained for other inert-gas atoms. The Huzinaga all electrons (10s,6p) and (12s,9p) basis sets contracted as [62111,411] by Dunning[26] and as [631111,52111] by McLean et al.[27] have been adopted for first- and second-row atoms, respectively (TZV option of the GAMESS code).[28] These basis sets were complemented with two "d" polarization functions and hereafter indicated as TZ2D (N: $\alpha_1 = 1.60$, $\alpha_2 = 0.40$; F: $\alpha_1 = 1.976$, $\alpha_2 = 0.425$; Ne: $\alpha_1 = 1.90$, $\alpha_2 = 0.475$; Cl: $\alpha_1 = 1.96$, $\alpha_2 = 0.36$; Ar: $\alpha_1 = 1.70$, $\alpha_2 = 0.425$; Xe: $\alpha_1 = 1.60$, $\alpha_2 = 0.40$).

To assess the influence of the basis set on the molecular properties of GdX_3, systematic improvements of TZ2D bases on both gadolinium and halogen atoms were analyzed (Table 1). Thus, the TZ2D bases were enlarged by adding the following in order: a "g" polarization function on Gd; an "sp" diffuse function on halogen; a second "g" polarization function on Gd; an "f" function on Gd; and an "f" polarization function on halogen. For halogens, standard exponents of diffuse "sp" and polarization "f" functions were adopted.[28] For gadolinium, Gaussian exponents were optimized by sets of UHF calculations. To check the reliability of shape-consistent pseudopotentials and basis sets presently adopted for gadolinium,[25a] additional calculations have been performed with use of the energy-consistent small-core pseudopotentials and basis sets developed by Dolg and Cao.[29] In these RECP the 4s, 4p, and 4d are included in the valence shell, thus the core-polarization effects are explicitly considered. Furthermore, the segmented contraction [5111111111,61111111,61111,5111,411] of the (14s13p10d8f6g)/[6s6p5d4f3g] atomic natural orbital basis set[29] (indicated as EXTENDED in Table 1) allows a great flexibility in the description of Gd−X bonds.

Cartesian Gaussian six d-type, ten f-type, and fifteen g-type basis functions were used. These introduce additional flexibility in the basis set because a single exponent α-d is associated with five d-type and one s-type functions, a single exponent α-f is associated with seven f-type and three p-type functions, while a single exponent α-g is associated with nine g-type, five d-type, and one-s type functions.

Electronic correlations were evaluated by adopting the computational performing MP2 treatment while high-order effects were accounted for through the coupled-cluster single and double excitations (CCSD) and by the CCSD corrected for the triples contribution by a perturbative fourth order calculation (CCSD(T)). Unless specifically noted otherwise, all valence electrons, including the semicore gadolinium 5s and 5p, are correlated. Adoption of extended basis sets, which produce single atom energy close to the Hartree−Fock limit, together with the MP2, CCSD, and CCSD(T) methods for electron correlation evaluation warrants an adequate description not only of anionic character for halogen atoms in GdX_3 molecules but also of weak intermolecular interactions with large dispersion contributions (van der Waals-type interactions) in $GdX_3 \cdot IG_m$ complexes.

The geometries of all the structures involved were fully optimized within the given symmetry constraints with use of gradient techniques at the UHF and MP2 levels (the adopted threshold on energy gradient was 0.00001 hartree/bohr). For the CCSD and CCSD(T) procedures, energy minimizations were achieved from a set of single-point energy calculations. The nature of the stationary points was determined by evaluations of the Hessian matrix and of associated harmonic vibrational frequencies. All the calculations were performed with the GAMESS code[28] while CCSD and CCSD(T) calculations were carried out with the G98 program.[30]

Anharmonic Vibrational Frequencies. Anharmonic vibrational frequencies were computed through the vibrational self-consistent field (VSCF) method and with its extension by second-order perturbation theory (PT2-VSCF).[31] In analogy to electronic structure theory methods, the vibrational wave function in the VSCF approximation is assumed to be the simple product function

$$\Psi_n(Q_1,...,Q_N) = \prod_{j=1}^{N} \psi_j^{(n_j)}(Q_j) \qquad (1)$$

where Q_j is the jth mass-weighted normal coordinate, n_j is the associated vibrational quantum number, and N is the number of vibration modes. Through this approximation the single-mode VSCF equations are derived:

$$\left[-\frac{1}{2}\frac{\partial^2}{\partial Q_j^2} + \bar{V}_j^{(n_j)}(Q_j)\right]\psi_j^{(n_j)}(Q_j) = \epsilon_j^{(n_j)}\psi_j^{(n_j)}(Q_j) \qquad (2)$$

where $\bar{V}_j^{(n_j)}(Q_j)$ is the effective VSCF potential for mode Q_j.

The eigenvalue eq 2 defines the variationally best modals $\psi_j^{(n_j)}$ for the quantum state $|n_1,...,n_N\rangle$. In addition to these modal wave functions, eq 2 yields a complete set of "virtual" modals for each mode. These virtual modals can be used as an expansion basis to perform a "configuration interaction" or perturbative calculations in analogy to methods developed in electronic structure theory. On the basis of standard second-order perturbation theory, Gerber et al.[31b] developed a general algorithm to correct VSCF energy for any vibrational levels (PT2-VSCF).

In the VSCF and correlation-corrected PT2-VSCF approaches the multidimensional integrals are reduced to one- and two-dimensional integrals assuming that potential function can be represented by including (in addition to separable, single-mode terms) only interactions between pairs of normal modes, i.e.

$$V(Q_1,...,Q_N) = \sum_{j=1}^{N} V_j(Q_j) + \sum_i \sum_{i<j} V_{ij}(Q_i,Q_j) \qquad (3)$$

The computation of integrals can be efficiently done by using a grid representation for $V_{ij}(Q_i,Q_j)$.

The grid step is computed by the simple relation

$$\mathrm{STEP} = \frac{\mathrm{QRANGE}}{(\mathrm{NGRID}-1)\sqrt{\omega_j}} \qquad (4)$$

where NGRID is the number of grid points (usually equal to 16) to be computed along each harmonic normal mode and along each pair of modes, ω_j is the harmonic frequencies of the jth mode, and QRANGE is a constant equal to 4.

In this way, PT2-VSCF ground-state vibrational energy ($n = 0$) and energy excited levels selecting $n = 1, 2, 3, ...$ can be obtained and hence wavenumbers of anharmonic fundamentals ($n \rightarrow n+1$, $n = 0$) and hot bands ($n \rightarrow n+1$, $n \geq 1$) for all vibrational modes.

In principle, the algorithm implemented on the GAMESS code[28] can compute energy levels with vibrational numbers up to the value [(NGRID/2) − 1], which for NGRID = 16 is 7. However, for high vibrational quantum numbers, the boundary of the grid defined by eqs 3 and 4 is approached or surpassed and actually only the energy of low vibrational states can be obtained (up to $n = 3$ and 5 for GdF_3 and $GdCl_3$, respectively). The presently investigated molecules are characterized by very small vibrational energy separations, thus levels with high quantum numbers are populated at the experimental conditions. Therefore, it is useful to explore excited states with high vibrational quantum numbers. To solve this difficulty we doubled the grid interval (QRANGE = 8 in eq 4) and the number of grid points (NGRID = 32) to maintain a high accuracy. A 16 point grid was used for the MP2 potential (3936 single-point energy calculations) with the default QRANGE interval, while a 32 point grid (15552 single points of energy) with a double interval was adopted for UHF.

Thermal Average Geometrical Parameters. A rigorous theoretical analysis of thermal average geometrical parameters would require the evaluation of the expectation value of these observables on the "exact" vibrational eigenstates which can be obtained through six-dimensional variational calculations by using a Hamiltonian expressed in curvilinear coordinates.[32] In this study, by means of a simple one-dimensional treatment, we focus our attention only on the vibrational modulation effect on the geometrical parameters of the molecules due to the inversion and the symmetric stretching motions (the two A_1 symmetry modes in C_{3v}).[33]

CHART 1

The large-amplitude out-of-plane bending motion was analyzed in the framework of the so-called distinguished coordinate approach whereby the path for the one-dimensional motion is obtained through an optimization of all the other geometrical parameters for selected values of a single distinguished coordinate.[34] For the description of the inversion motion the bond angle X−Gd−X, Θ, was chosen as the representative coordinate while the R_{Gd-X} bond length was optimized retaining the 3-fold axis. In this way, the out-of-plane motion description takes into account implicitly the coupling with symmetric stretching in an effective fashion. In the description of the symmetric stretching mode, the bond length, R_{Gd-X}, was chosen as the representative coordinate. Next, the inversion and symmetric stretching paths were described in terms of the distance s, evaluated in mass weighted Cartesian coordinates, along the above paths, s being set to zero at a suitable reference configuration.

Since the path variable s is measured in the space of the mass weighted Cartesian coordinates, the Schrödinger equation for the system is formally equivalent to that governing the motion of a particle with unit mass in a one-dimensional space

$$[T_N(s) + V_{\mathrm{eff}}(s)]\psi^{(n)}(s) = \epsilon^{(n)}\psi^{(n)}(s) \qquad (5)$$

The variational solution of the effective one-dimensional problem is obtained by using evenly spaced cubic b-spline functions both to interpolate the potential energy function and as a basis function.[35] In this way two advantages are obtained: (i) there is no need to choose a functional form for the potential energy function that must fit the ab initio data and (ii) only analytical integrals are involved, irrespective of the more or less complicated form of potential, kinetic, and eventual coupling terms.[36] Once the nth eigenstates corresponding to the energy eigenvalues $\epsilon^{(n)}$ are known, the expectation value $\langle O\rangle^{(n)}$ of any observable is given by

$$\langle O\rangle^{(n)} = O_{\mathrm{ref}} + \langle\psi^{(n)}(s)|\Delta O(s)|\psi^{(n)}(s)\rangle \qquad (6)$$

where O_{ref} is the value of the observable at the reference configuration, and $\Delta O(s)$ is its variation as a function of the progress variable s which, in the present treatment, is also represented as cubic b-spline fitting.[33]

By assuming a Boltzmann population of the eigenstates, the temperature dependence of the observable $\langle O\rangle_T$ can finally be obtained:

$$\langle O\rangle_T = \frac{\sum_n \langle O\rangle^{(n)} \exp[(\epsilon^{(0)} - \epsilon^{(n)})]/k_B T}{\sum_n \exp[(\epsilon^{(0)} - \epsilon^{(n)})]/k_B T} \qquad (7)$$

where k_B is the Boltzmann constant.

Results and Discussion

Gas-Phase Equilibrium and Thermal Average Structures. GdX_3 molecules can assume alternatively planar trigonal D_{3h} or pyramidal trigonal C_{3v} equilibrium structures. The present

TABLE 2: Calculated Equilibrium Bond Lengths R_e (Å), Bond Angles Θ_e (deg), Harmonic Vibrational Frequencies (cm^{-1}), and IR (km/mol) and Raman ($Å^4$/Amu) Intensities of Isolated GdF_3 and $GdCl_3$ Molecules

				ν_1			ν_2			ν_3			ν_4		
	computational level	R_e	Θ_e	ω	IR	Raman	ω	IR	Raman	ω	IR	Raman	ω	IR	Raman
GdF_3	TZ2D/UHF	2.059	120	565.7	0.	1.36	41.1	95.2	0.	550.7	226.1	0.01	135.3	24.3	0.23
	TZ2D/MP2	2.048	118.5	565.2	4.5	4.21	36.9	77.5	0.02	551.3	208.6	0.01	132.7	17.3	0.52
	TZ2D/CCSD(T)	2.051	119.0												
	TZ2DG/MP2	2.043	117.9	575.5			43.8			560.0			132.9		
	TZ2DG+/MP2	2.044	118.0	571.6			43.1			554.2			132.2		
	TZ2D2G+/MP2	2.045	120	569.9			22.2			554.4			124.4		
	TZ2D2GF+/MP2	2.047	120	564.4			13.7			549.4			125.7		
	TZ2D2G2F+/MP2	2.045	119.9	566.1			6.5			550.6			125.7		
	TZ2D2G2F+/MP2-AE[a]	2.045	119.9	566.1			4.7			550.5			125.1		
	EXTENDED/CCSD-AE	2.041	120												
$GdCl_3$	TZ2D/UHF	2.524	120	323.6	0.	3.29	42.5	44.5	0.	339.9	136.1	0.08	77.1	7.9	1.35
	TZ2D/MP2	2.486	120	331.6	0.	7.03	24.2	37.9	0.	353.2	126.5	0.01	74.6	5.0	2.14
	TZ2D/CCSD(T)	2.496	120												
	TZ2DG/MP2	2.468	120	336.5			13.7			358.6			74.9		
	TZ2DG+/MP2	2.469	120	335.7			13.2			357.1			74.9		
	TZ2D2G+/MP2	2.467	120	337.2			25.7			357.7			70.4		
	TZ2D2GF+/MP2	2.475	120	330.3			27.0			353.1			72.4		
	TZ2D2G2F+/MP2	2.468	120	335.3			25.1			358.6			73.0		
	TZ2D2G2F+/MP2-AE[a]	2.465	120	335.6			23.7			360.6			73.3		
	EXTENDED/CCSD-AE[a,b]	2.474	120												

[a] All electrons were correlated. [b] Pure "d", "f", and "g" spherical harmonics were used. Excitations into 15 and 27 highest energy virtual orbitals were excluded for the GdF_3 and $GdCl_3$ molecules, respectively.

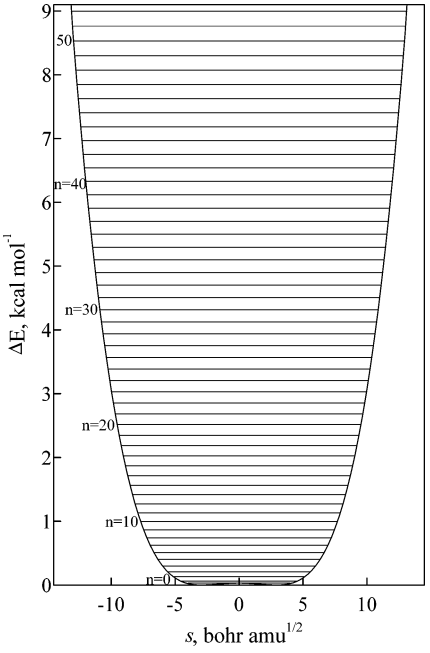

Figure 1. Potential energy curve along the out-of-plane bending motion for the GdF_3 molecule as a function of the path variable *s*. The curve (TZ2D/MP2) has been obtained by fixing the Θ angle to selected values and optimizing the R_{Gd-F} distance.

data (Table 2) indicate that at the TZ2D/UHF level the planar structure is favored for both GdX_3 structures. When electron correlation effects are included at both the TZ2D/MP2 and TZ2D/CCSD(T) levels, the GdF_3 planar structure becomes unstable toward the out-of-plane distortion and the pyramidal geometry is energetically favored (Figure 1). The $GdCl_3$ structure does not incur the out-of-plane instability as the theory level increases, therefore the planar geometry represents the equilibrium structure. However, in analogy to the GdF_3 molecule, on passing from UHF to correlated MP2 and CCSD(T) methods, the potential energy along the out-of-plane bending becomes more flat and the associated ν_2 vibrational frequency is considerably reduced (Table 2). Such lowering of the potential walls for the inversion motion can be explained by the balancing between the interelectronic repulsion and correlation energy that occurs when the halogen atoms, moving away from the D_{3h} molecular plane, come closer.

In view of the extreme fluxionality of these molecules, additional calculations improving the basis set were performed at the MP2 level to test the reliability of the TZ2D basis set. With all basis sets presently considered (Table 1) the equilibrium structure of $GdCl_3$ is always found to be planar even though the curvature around the minimum changes substantially as is evident from the harmonic frequency of the ν_2 out-of-plane bending (Table 2). Thus, the inclusion of one "g" polarization function on Gd reduces the curvature (ν_2 diminishes) while the inclusion of the second "g" polarization function on Gd makes the curve steeper and ν_2 rises becoming close to the value obtained at the TZ2D/MP2 level. The inclusion of an additional "f" function on Gd slightly increases the tendency toward a planar structure. Basis set improvements on halogens have negligible effects for the potential surface along the out-of-plane bending of the $GdCl_3$ molecule. Analogously, for GdF_3 the inclusion of one "g" polarization function on Gd enhances the pyramidalization tendency, while the second "g" function leads to a planar structure. However, the MP2 calculation with the best basis set leads to a slightly bent structure for GdF_3. On the other hand, it should be noted that the energy gain upon bending the GdF_3 is of the same magnitude (<0.001 kcal/mol at the TZ2D2G2F+/MP2-AE level) as the zero point energy associated with the ν_2 out-of-plane mode. Therefore, it is reasonable to think that atoms are not confined in the C_{3v} well and the GdF_3 molecule may be classified as a quasiplanar structure. These conclusions are supported by CCSD calculations adopting the relativistic small-core pseudopotential and extended basis set on the gadolinium atom (Table 2). These data point to a planar structure for both GdF_3 and $GdCl_3$ molecules.

The present results are similar to ab initio data reported by Cundari et al.[18] and Hirao et al.,[22] who used the same RECP and basis set contraction on the gadolinium atom and a smaller basis set on halogen atoms (6-31G*). However, having neglected electron correlation effects, they predicted planar structures for both GdX_3 molecules. Joubert et al.,[20b] adopting the Stuttgart

RECP (4f orbitals are treated as core orbitals) and MP2, reported a planar structure for $GdCl_3$ and a slightly pyramidal structure for GdF_3, thus indicating that ab initio values are less sensitive to computational parameters. The same authors, by contrast, reported pyramidal structures for both GdF_3 ($\Theta = 113.6°$) and $GdCl_3$ ($\Theta = 118.8°$) when the DFT-B3LYP approach was used.[20a] In addition, various sets of data on GdX_3, based on DFT methodologies, were given by Adamo et al.[19] They predicted more pyramidal structures with bond angles spread in the range 113.9−117.7° for GdF_3 and 118.7−120.0° for $GdCl_3$, depending on the exchange and correlation potentials adopted. Such results clearly indicate that a rigorous evaluation of the correlation energy and nonlocal exchange integrals is mandatory. It is well-known that DFT-based methodologies overestimate correlation effects and hence pyramidal structures are artificially favored.[37]

Electron correlation effects also appear critical in the bond distance estimation, hence a 0.011 and 0.038 Å shortening is observed on passing from UHF to MP2 for GdF_3 and $GdCl_3$, respectively. Conversely, an elongation of 0.003 Å for GdF_3 and 0.010 Å for $GdCl_3$ is observed on passing from MP2 to CCSD(T) when the TZ2D basis set is adopted. Basis sets larger than the TZ2D always lead to shorter bond lengths. This effect is more pronounced for $GdCl_3$ than GdF_3 and the maximum contractions are 0.022 and 0.01 Å, respectively. These findings show that, on increasing the theoretical level, the variation of the Gd−X distance is lower for X = F than for X = Cl.

The comparison of theoretical and experimental geometrical parameters is not a simple task. In fact, the equilibrium structure generally derived in electronic structure computations corresponds to the minimum on the Born−Oppenheimer potential energy surface. In ED studies the thermal average geometry is derived, i.e., the distance between atoms averaged over all vibrations of all molecules present in the gas phase at a given temperature.[1] Thus, both the thermal average Gd−X (average bond length R_g) and X···X distances are directly measured while the X−Gd−X bond angle is indirectly derived (virtual average angle Θ_{vg}). The symmetry of the thermal average geometry of lanthanide trihalides may be quite different from the molecule equilibrium structure due to the soft deformation modes as a consequence of the so-called "shrinkage effect". For example, in a recent experimental gas-phase ED study of $GdCl_3$ at ∼1160 K, a C_{3v} structure ($R_g = 2.474(5)$ Å and $\Theta_{vg} = 117.0(1.1)°$) was obtained.[15a] However, applying a dynamic model to take into account the anharmonicity for the out-of-plane bending vibration, a planar equilibrium structure was derived, in full agreement with our results.

A rigorous theoretical analysis of R_g and Θ_{vg} is beyond the capabilities of our present computational tools. However, by means of the simple effective one-dimensional treatment, described in the computational section, vibrational modulation effects of out-of-plane bending and symmetric stretching modes on the geometrical parameters can be easily included. Despite the simplicity of the adopted model, important information has been derived. Figure 1 reports the potential energy curve for the out-of-plane motion of GdF_3 (the single-well curve for $GdCl_3$ is not reported). The potential has a rather flat and anharmonic form and resembles a "square-well" with a flat bottom and steep walls at the edge, typical of many modes with very low vibrational frequencies. For both GdF_3 and $GdCl_3$ systems, the decrease of the bond angle is accompanied by a gradual reduction of the R_{Gd-X} distance. Indeed, a bending of 15° implies a bond length shortening of ∼0.02 Å for both GdX_3 molecules.

TABLE 3: Calculated TZ2D/MP2 Average Bond Lengths *R* (Å) and Bond Angles (deg) of GdF_3 and $GdCl_3$ over the Out-of-Plane and the Symmetric Stretching Vibrations at Various Temperature (K) Along with Experimental Average Structural Parameters (R_g and Θ_{vg}) and Equilibrium Geometrical Data (in parentheses) for Comparison

	computation			experiment[15]	
temp	$\langle R\rangle_T$[a]	$\langle\Theta\rangle_T$[a]	$\langle R'\rangle_T$[b]	R_g	Θ_{vg}
GdF_3	(2.048)	(118.5)	(2.048) [2.051]		
0	2.049	119.2	2.049 [2.052]		
20	2.048	119.0	2.049 [2.052]		
298.15	2.046	117.6	2.049 [2.053]		
500	2.046	117.0	2.050 [2.053]		
1000	2.044	116.0	2.051 [2.054]		
1830	2.042	114.8	2.053 [2.057]	2.053(3)	108.4(2.4)
$GdCl_3$	(2.486)	(120)	(2.486) [2.496]		(120)[c]
0	2.486	119.8	2.487 [2.497]		
20	2.486	119.8	2.487 [2.497]		
298.15	2.483	118.4	2.487 [2.497]		
500	2.482	117.7	2.488 [2.498]		
1000	2.481	116.5	2.490 [2.500]		
1160	2.480	116.2	2.490 [2.501]	2.474(5)	117.0(1.1)

[a] Thermal average structure over the out-of-plane vibration. [b] Thermal average distance over the symmetric stretching vibration. The CCSD(T) data are reported in brackets. [c] Value estimated from ED data.[15a]

By assuming a Boltzmann population of the eigenstates (Figure 1) for the large-amplitude inversion motion, the thermal average angles $\langle\Theta\rangle_T$ and the thermal average bond lengths $\langle R\rangle_T$ were computed at various temperatures (Table 3). The $\langle\Theta\rangle_T$ values obtained for the $GdCl_3$ molecule are always lower than the equilibrium bond angle even at 0 K, thus vibrational modulation effects lead to C_{3v} structures for $GdCl_3$. For the vibrational ground state the maximum of probability distribution is located at $\Theta = 120°$, therefore, the average bond angle is very close to the planar equilibrium structure. Conversely, for excited states, absolute maxima move toward the potential walls (smaller bond angles) implying a significant reduction of average bond angles on increasing the temperature.

For the GdF_3 molecule, the exclusive population of the lowest vibrational level (0 K) increases the bond angle leading to an average structure less pyramidal than that of the equilibrium, i.e., the two maxima of vibrational probability distribution for ground state "move" closer to D_{3h} geometry. On populating high excited vibrational levels more pyramidal structures than the equilibrium one are found ($\langle\Theta\rangle_T$ decreases). The resulting MP2 thermal average distances $\langle R\rangle_T$, computed along the out-of-plane motion, slightly decrease with respect to the R_e and at the experimental ED temperature a shortening of 0.006 Å is observed for both systems.

The potential energy profile associated with the symmetric stretching mode of GdF_3 is reported in Figure 2 (the curve for $GdCl_3$ is not reported). The curve shows the classical asymmetric form with respect to the equilibrium position, while the vibrational levels crowd more closely together with increasing vibrational number *n*. The probability distributions of each vibrational level are slightly skewed such that they have greater magnitude on the side of the well corresponding to bond stretching. This skewing toward increasing R_{Gd-X} implies that the average internuclear position augments with increasing value of the quantum number *n*. Thus, at high temperature, when vibrational states with high quantum numbers are significantly populated (up to $n = 5$ for GdF_3 and up to $n = 7$ for $GdCl_3$), the resulting MP2 thermal average distance along the symmetric stretching mode $\langle R'\rangle_T$ is slightly longer (∼0.004 Å, Table 3) than R_e for both molecules. Another important aspect emerging

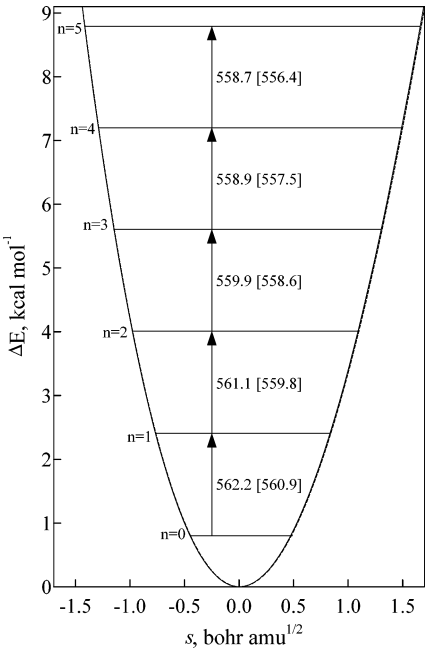

Figure 2. Potential energy curves along the symmetric stretching motion for the GdF_3 molecule as a function of the path variable *s*. The curves (TZ2D/MP2, solid line; and TZ2D/CCSD(T), dashed line) have been obtained by changing the R_{Gd-F} distance at the Θ_e equilibrium angle. MP2 and CCSD(T) (in brackets) vibrational spacing between adjacent levels are also reported.

from Figure 2 is the vibrational step reduction for the lowest vibrational levels ($\omega_{1-2} - \omega_{0-1} = -1.1$; $\omega_{2-3} - \omega_{1-2} = -1.2$; $\omega_{3-4} - \omega_{2-3} = -1.0$; $\omega_{4-5} - \omega_{3-4} = -0.2$ cm^{-1}). Instead, for high-lying levels the vibrational spacing increases ($\omega_{5-6} - \omega_{4-5} = 2.4$ cm^{-1}). This is due to the incorrect form of the right-side MP2 potential curve (long internuclear distances). In fact, it is well-known that the HF single determinant wave function for a molecule near its equilibrium geometry is the dominant term in the total configuration interaction expansion. The other terms represent corrections to the wave function, their coefficients are individually small, and generally they are well represented by second-order perturbation theory. Upon moving far from equilibrium structures on the right side of the curve, several configurations are necessary to account for correlation between the pairs of electrons involved in partial bond dissociation. Thus, more sophisticated wave functions in describing the electronic correlation are required to calculate the potential surfaces far from equilibrium. The CCSD(T) method incorporates parts of the CI quadruple excitation terms in the variational CCSD procedure in addition to single and double excitations. Further, triple excitations are included throughout perturbative treatment. Therefore, in principle it can partially solve the classical shortcoming of single-determinant electronic wave functions in describing bond breaking.

The CCSD(T) potential energy curves along the symmetric stretching and associated anharmonic vibrational levels are reported in Figure 2. The MP2 and CCSD(T) curves on the side of the well corresponding to the bond contraction almost overlap, while on the other side of the well the CCSD(T) curve lies at lower energy than the MP2 one and the difference is more pronounced at high values of R_{Gd-F} (at $s = 1.7$ bohr amu$^{1/2}$ the $\Delta E_{MP2} = 9.15$ and $\Delta E_{CCSD(T)} = 9.05$ kcal/mol). The anharmonic vibrational frequencies derived from the CCSD(T) curve are close to that obtained with the MP2 and the reduction of anharmonic frequencies, upon increasing vibrational quantum number, on the CCSD(T) well ($\omega_{1-2} - \omega_{0-1} = -1.1$; $\omega_{2-3} - \omega_{1-2} = -1.2$; $\omega_{3-4} - \omega_{2-3} = -1.1$ cm^{-1}), is identical with that obtained with the MP2 well for low-lying levels. Conversely, the reduction of anharmonic frequencies differs for high-lying states ($\omega_{3-4} - \omega_{4-5} = -1.1$; $\omega_{4-5} - \omega_{5-6} = -0.9$ cm^{-1}). These data clearly suggest that the CCSD(T) approach better reproduces the behavior of the curve on the side corresponding to bond stretching and the vibrational step reduction is in agreement with the chemical intuition. The obvious consequence is that the adoption of the CCSD(T) wave function leads to slight elongation (~0.005 Å, Table 3) of the bond distance due to the vibrational effects.

TABLE 4: Calculated TZ2D/UHF and TZ2D/MP2 (in parentheses) Anharmonic PT2-VSCF Vibrational Transitions (cm^{-1}) for the GdF_3 in the Gas Phase[a]

	ν_1		ν_2		ν_3		ν_4	
	ω	$\Delta\omega$	ω	$\Delta\omega$	ω	$\Delta\omega$	ω	$\Delta\omega$
harmonic	565.7		41.2		550.7		135.3	
	(565.2)		(36.9)		(551.3)		(132.7)	
0 → 1	562.2		44.7		545.9		134.9	
	(561.3)		(34.3)		(545.5)		(131.7)	
1 → 2	561.4	−0.8	47.7	3.0	543.8	−2.1	134.7	−0.2
	(558.5)	(−2.8)	(40.4)	(6.1)	(543.1)	(−2.4)	(131.5)	(−0.2)
2 → 3	560.7	−0.7	51.2	3.5	541.6	−2.2	134.5	−0.2
	(557.5)	(−1.0)	(44.8)	(4.4)	(540.5)	(−2.6)	(131.3)	(−0.2)
3 → 4	560.1	−0.6	53.9	2.7	539.4	−2.2	134.4	−0.1
4 → 5	559.6	−0.5	56.2	2.3	537.2	−2.2	134.3	−0.1
5 → 6	559.3	−0.3	58.0	1.8	535.1	−2.1	134.2	−0.1

[a] $\Delta\omega = \omega_{n+1\to n+2} - \omega_{n\to n+1}$ (n = vibrational quantum number).

The calculated thermal average bond angles along the out-of-plane motion, $\langle\Theta\rangle_T$, at the experimental temperatures are in reasonable agreement with the Θ_{vg} parameters obtained from gas-phase ED measurements for both molecules (Table 3).[15] The comparison of theoretical thermal average bond distance and the experimental R_g parameter requires a deeper analysis.

At the best computational level presently considered (TZ2D2G2F+/MP2-AE and EXTENDED/CCSD-AE) the equilibrium bond length of the GdF_3 molecule is ~0.01 Å shorter than the experimental R_g. For the $GdCl_3$ molecule R_e is 0.009 Å shorter than R_g at the TZ2D2G2F+/MP2-AE level while the two values are coincident at the EXTENDED/CCSD-AE level. Assuming simple additive effects due to the thermal vibrational modulation discussed above, the bond length shortening due to the out-of-plane bending (0.006 Å) would be compensated by the lengthening due to the symmetric stretching motion (0.005 Å). Therefore, the computed thermal average bond length over these two modes is still underestimated with respect to experimental data. The double-degenerate in-plane bending mode shows a very small anharmonicity (vide infra, Tables 4 and 5), therefore, its effect on thermal structure should be very small. Conversely, the double-degenerate asymmetric stretching presents a considerable "negative" anharmonicity about two times that computed for symmetric stretching (Tables 4 and 5) and a substantial bond lengthening (at least 0.01 Å or even higher) should occur when the structure is averaged over this mode. Summarizing, we may conclude that the bond distance averaged over all vibrations should be greater than the equilibrium bond distance by ~0.01 Å. An addition of 0.01 Å to the presently best computed R_e (TZ2D2G2F+/MP2-AE and EXTENDED/CCSD-AE) of GdF_3 leads the theoretical thermal average structure very close to that measured by ED, within experimental error (2.055 and 2.051 Å, respectively, vs 2.053(3) Å). For $GdCl_3$ the estimated R_g parameter (R_e + 0.01 Å) is very close to experimental data at the TZ2D2G2F+/MP2-AE level (2.475 Å vs 2.474(5) Å) while it is slightly overestimated at the EXTENDED/CCSD-AE level (2.484 Å vs 2.474(5) Å).[15]

TABLE 5: Calculated TZ2D/UHF and TZ2D/MP2 (in parentheses) Anharmonic PT2-VSCF Vibrational Transitions (cm^{-1}) for the $GdCl_3$ in the Gas Phase[a]

	ν_1		ν_2		ν_3		ν_4	
	ω	$\Delta\omega$[a]	ω	$\Delta\omega$	ω	$\Delta\omega$	ω	$\Delta\omega$
harmonic	323.6		42.5		339.9		77.1	
	(331.6)		(24.2)		(353.2)		(74.6)	
0→1	322.3		42.9		337.8		77.1	
	(330.3)		(25.9)		(351.1)		(74.7)	
1→2	321.9	−0.4	43.3	0.4	337.0	−0.8	77.2	0.1
	(329.9)	(−0.4)	(27.1)	(1.2)	(350.1)	(−1.0)	(74.6)	(−0.1)
2→3	321.5	−0.4	43.7	0.4	336.2	−0.8	77.2	0.0
	(329.6)	(−0.3)	(28.8)	(1.7)	(349.2)	(−0.9)	(74.6)	(0.0)
3→4	321.1	−0.4	44.2	0.5	335.5	−0.7	77.3	0.1
	(329.1)	(−0.5)	(30.3)	(1.5)	(348.3)	(−0.9)	(74.7)	(0.1)
4→5	320.8	−0.3	44.7	0.5	334.9	−0.6	77.4	0.1
	(328.5)	(−0.6)	(31.4)	(1.1)	(347.2)	(−1.1)	(74.7)	(0.0)
5→6	320.6	−0.2	45.2	0.5	334.4	−0.5	77.5	0.1
6→7	320.5	−0.1	45.7	0.5	334.2	−0.2	77.8	0.3
7→8	320.7	0.2	46.4	0.7	334.2	0.0	77.9	0.1

[a] $\Delta\omega = \omega_{n+1\rightarrow n+2} - \omega_{n\rightarrow n+1}$ (n = vibrational quantum number).

Gas-Phase Harmonic and Anharmonic Vibrational Frequencies. Calculated harmonic vibrational frequencies and related IR and Raman intensities at the UHF and MP2 levels are listed in Table 2. Normal mode IR intensities indicate that for D_{3h} symmetry molecules, asymmetric stretching (ν_3), out-of-plane (ν_2), and in-plane (ν_4) bending are IR active ($\nu_3 \gg \nu_2 > \nu_4$). The symmetric stretching ν_1 becomes active only for GdF_3 (in C_{3v} symmetry) with a very weak intensity. The weak (or absent) ν_1 and ν_4 IR absorptions correspond, in contrast, to the most intense bands in Raman measurements while the ν_2 and ν_3 would be very weak or absent. These data clearly suggest that both spectroscopic measurements are required for a clear and univocal vibrational frequency characterization.

Harmonic vibrational frequencies show that symmetric and asymmetric stretching and scissors-type bending of both GdF_3 and $GdCl_3$ slightly depend on adopted methods (the maximum difference observed is 11 cm^{-1}). More pronounced variations are observed for the ν_2 out-of-plane bending because of the strong potential energy modification along this normal mode.

The potential energy curves for the out-of-plane ν_2 mode of both molecules have a rather flat and anharmonic form (Figure 1) and in the low potential energy region (≤4 kcal/mol) they can be fitted adequately in terms of changes in bond angle ($\Delta\Theta$) only by an even tenth-degree polynomial

$$\Delta E_{GdF3} = 0.0199 - 0.0109(\Delta\Theta)^2 + 0.0015(\Delta\Theta)^4 - (3.126 \times 10^{-5})(\Delta\Theta)^6 + (2.339 \times 10^{-7})(\Delta\Theta)^8 - (5.346 \times 10^{-10})(\Delta\Theta)^{10} \quad (8)$$

$$\Delta E_{GdCl3} = 0.0756(\Delta\Theta)^2 - 0.00339(\Delta\Theta)^4 + (7.083 \times 10^{-5})(\Delta\Theta)^6 - (5.304 \times 10^{-7})(\Delta\Theta)^8 + (1.213 \times 10^{-9})(\Delta\Theta)^{10} \quad (9)$$

The constant term is equal to zero for the single-well potential while it is a positive number for the double-well potential. It is important to note that there is an alternation of sign in polynomial coefficients on increasing the exponent of the terms, i.e., there is a poor convergence in the Taylor expansion of the potential because of the strong curvilinear character of the out-of-plane motion. Therefore, it is not simple to predict a priori the behavior of the energy levels on increasing the vibrational quantum number. The negative sign for the quadratic term in the GdF_3 energy polynomial suggests that the harmonic vibrational frequency is not representative of the entire curve.

The potential energy curves obtained along the ν_1 and ν_3 stretching modes and for the ν_4 in-plane bending mode (Figure 2 for the ν_1 of GdF_3) are close to the quadratic form, thus harmonic frequencies are reasonable. For example, the TZ2D/MP2 potential energy curves for the symmetric stretching ν_1 mode of both molecules can be fitted adequately (up to 4 kcal/mol) in terms of changes in bond distance (ΔR) by a third-degree polynomial

$$\Delta E_{GdF3} = 768.408(\Delta R)^2 - 1023.4(\Delta R)^3 \quad (10)$$

$$\Delta E_{GdCl3} = 492.405(\Delta R)^2 - 583.512(\Delta R)^3 \quad (11)$$

The negative sign of the cubic term suggests that the vibrational frequencies of hot transitions are lower than the fundamental frequency, indeed pointing to a "positive" anharmonicity constant.

Calculated PT2-VSCF anharmonic fundamentals and hot bands for all vibrational modes are listed in Tables 4 and 5 for GdF_3 and $GdCl_3$, respectively. The tables also report the vibrational difference $\Delta\omega$ between adjacent vibrational transitions starting from the fundamental ($\Delta\omega = \omega_{n+1\rightarrow n+2} - \omega_{n\rightarrow n+1}$; n = vibrational quantum number). The adopted PT2-VSCF procedure does not preserve symmetry, and therefore, the degenerate vibrational frequencies are not exactly degenerate at the PT2-VSCF level. However, differences on computed fundamental and hot bands are negligible for the degenerate ν_4 modes (<0.2 cm^{-1}). Small differences are observed also for the couple of ν_3 modes (<1 cm^{-1}) for the fundamental or for hot bands characterized by low vibrational number while they increase (up to 3 cm^{-1}) for transitions involving levels with high quantum numbers in the case of $GdCl_3$ employing the UHF wave function. In all cases average values are reported in Tables 4 and 5.

On passing from harmonic to fundamental and to hot transitions of both molecules it can be seen that anharmonicities are small for all normal modes but ν_2. This is in agreement with the almost quadratic potential energy surface found for the ν_1, ν_3, and ν_4 modes and with strong deviations from quadratic curves for the ν_2 mode (Figure 1 and eqs 8 and 9) discussed above. In all cases, absolute value differences are more pronounced for GdF_3 normal modes than for $GdCl_3$. For both molecules the frequencies of stretching modes (ν_1 and ν_3) decrease slightly on passing from harmonic to fundamental and to hot transitions thus indicating a small "positive" anharmonicity constant. For the ν_4 scissors-type bending, harmonic, fundamental, and hot transitions are almost coincident indicating a "pure" harmonic potential. The frequency of the inversion mode (ν_2) increases as the quantum number of levels involved in the transition increases. This suggests a "negative" anharmonicity constant. Thus, the UHF computed 5→6 hot band frequency for ν_2 is ∼30% greater than the fundamental 0→1 for GdF_3, while the 7→8 hot band frequency is 8% greater than the fundamental one for $GdCl_3$. Anharmonicities are more pronounced when the MP2 method is adopted in computing potential grids, thus the 2→3 hot band frequency for ν_2 is ∼30% greater than the fundamental 0→1 for GdF_3 while the 4→5 hot band frequency is ∼21% greater than the fundamental one for $GdCl_3$. These data are in agreement with effective one-dimensional frequencies previously discussed (vide supra). In fact, computation of high-lying states (Figure 1) reveals that the energy difference between adjacent vibrational levels

increases as the vibrational number grows and the 50→51 hot band transition frequency reaches the value of 81.0 and 50.8 cm^{-1} for GdF_3 and $GdCl_3$, respectively.

Hot band frequencies of both ν_1 symmetric and ν_3 asymmetric stretching decrease upon increasing the quantum number and the reduction is more pronounced for the asymmetric one. As found for frequencies computed with the effective one-dimensional method (Figure 2) the vibrational levels do not crowd more closely together for the highest energy levels. These data confirm the inability of UHF and the "partial accuracy" of MP2 methods in the computation of potential energy in regions far from the equilibrium structure. Therefore, the adoption of sophisticated wave functions becomes mandatory to obtain the correct behavior of high-lying levels as shown by the one-dimensional data discussed above.

Considering the data of Tables 2 and 5, we can critically analyze the high-temperature (1350 K) gas-phase IR spectrum of $GdCl_3$. The IR spectrum of $GdCl_3$ shows two broad bands: the first in the 300−360 cm^{-1} range that exhibits a flattened band shape on the low-frequency wing and the second in the 35−85 cm^{-1} range. For the trigonal planar D_{3h} structure only the ν_2, ν_3, and ν_4 modes are active in the IR while the ν_1 is inactive. Therefore, the band located approximately at 335 cm^{-1} is assigned to the ν_3 normal mode while the band envelop in the range 35−85 cm^{-1} contains absorptions of both ν_2 and ν_4 modes. For the $GdCl_3$ symmetric top molecule, the ν_3 is a perpendicular vibration and gives rise to many sets of P, Q, and R unresolvable branch lines which produce a consistent peak broadening. However, this is not the only reason for the presence of such a large absorption. In fact, due to the anharmonicity the computed hot bands (Table 5) are shifted one by one by 1 cm^{-1} thus a significant absorption enlargement occurs. In addition, due to the fact that at high levels the population is reduced (for the ν_3 mode, Boltzmann population at 1350 K of the nine lowest states relative to the fundamental one are:1.00, 0.70, 0.50, 0.35, 0.25, 0.17, 0.12, 0.09, and 0.06), the associated hot band intensities decrease thus rendering the peak asymmetric in agreement with the absorption band shape observed in the experimental IR spectrum.

The ν_2 is a parallel vibration and each transition gives rise to a single set of P, Q, and R branches. However, as discussed above, this mode suffers a strong negative anharmonicity and levels up to the vibrational quantum number 50 are significantly occupied thus giving rise to tens of PQR structures separated by the anharmonic hot band shift. All computational data suggest a large dispersion of vibrational transitions. Indeed, the MP2/PT2-VSCF lowest five transitions spread in the range 25.9−31.4 cm^{-1}, the UHF/PT2-VSCF lowest eight transitions spread in the range 42.9−46.4 cm^{-1}, while the lowest fifty transitions, computed by using the effective one-dimensional approach at the MP2 level, spread in the range 25.6−50.8 cm^{-1}. This large diffusion of vibrational transitions allows the explanation of the large band (starting from ∼35 up to ∼85 cm^{-1}) observed in the gas-phase IR spectrum. The ν_4 falls in the same region of the ν_2 absorption, and it is a perpendicular vibration that gives rise to complex PQR branch lines. The ν_4 mode is much less intense than the ν_2 mode and suffers from very small anharmonicity, therefore, it should give a "sharp" signal centered at ∼75 cm^{-1} superimposed to the main ν_2 band. In fact, the large band in the 35−85 cm^{-1} range associated with the ν_2 mode shows a shoulder at ∼77 cm^{-1} probably due to the ν_4 absorption.

Because of the very high temperature required to obtain molecular vapors, the gas-phase IR spectrum of GdF_3 has not been reported up to now and a detailed comparison of experimental and theoretical analysis is hampered. However, it is likely that the considerations made for $GdCl_3$ may be valid for the trifluoride analogue.

Geometry and Harmonic Vibrational Frequencies of Molecules Trapped in Inert-Gas Matrices. Vibrational spectroscopies of isolated reactive molecules in inert matrices at cryogenic temperatures have been largely applied to lanthanide trihalides. Both vibrational and rotational motions are quenched and resulting IR/Raman spectra are greatly simplified compared to those obtained in the gas phase at high temperature. Nevertheless, spectra interpretation is not a simple task. For example, while DeKock et al. deduced from IR and Raman (only for PrF_3) spectra the planar structure for LnF_3 molecules,[7] Hastie, Hauge, and Margrave, with independent IR measurements, pointed to a pyramidal structure for the same molecules.[6] On the other hand, there is growing experimental evidence indicating that host−guest interactions in matrices play a significant role in the molecular symmetry, geometrical parameters, and vibrational frequencies of floppy molecules.[3]

From a computational point of view the simulation of host−guest interactions is a challenging task and various treatments have been proposed.[38,39] In a simplified view two effects should be considered: (i) a local static interaction between the molecule and the neighbor matrix atoms which might lead to the formation of a "complex" and (ii) a nonlocal dynamic effect due to the coupling of extended solid vibrations and intramolecular modes.

In the solid state, GdF_3 assumes a distorted trigonal prism capped on all faces in which the cation coordination is 11 while for $GdCl_3$ the coordination group of the metal ion is a tricapped trigonal prism with nine approximately equidistant chlorine neighbors.[40] In stable monomeric complexes the gadolinium atom generally presents a high coordination number (>7) to obtain kinetic stabilization.[41] Gas-phase isolated GdX_3 species (coordination number = 3) are extremely reactive (special precautions must be adopted because of their high corrosive nature). The extraordinary Lewis acid character of gas-phase GdX_3 molecules suggests that interactions between GdX_3 and neighbor matrix atoms are substantial. In this perspective, we simulated matrix effects by considering complexes with one and two inert-gas atoms or molecules coordinated to gadolinium. This is admittedly a crude model; however, despite its simplicity, it can be seen that observed experimental spectroscopic features are well-reproduced at least at the qualitative level.

Figure 3 shows schematic representations of $GdX_3 \cdot IG$ and $GdX_3 \cdot IG_2$ (IG = Ne, Ar, Xe, and N_2) complex structures, while Table 6 collects geometrical parameters and complex formation energies ($GdX_3 + mIG \rightarrow GdX_3 \cdot IG_m + \Delta E$, $m = 1$ and 2) obtained at UHF and MP2 levels.

Complex formation energies at both UHF and MP2 levels, corrected for basis set superposition error (Table 6), indicate that inert-gas atoms (or molecules) strongly coordinate the metal and the bonding energy depends on inert-gas species. Some general features can be derived analyzing the data reported in Table 6.

(1) MP2 complexation energies are considerably greater than those obtained with the UHF wave function. This indicates that the electron correlation energy is extremely important in computing weak van der Waals interactions (ion−induced-dipole) between molecules and host−matrix.

(2) The BSSE is small but not negligible for both MP2 and UHF methods.

(3) The coordination energy of two inert-gas atoms (or molecules) is almost double that obtained for the coordination of a single species. Thus, the high Lewis acidity of GdX_3 is

TABLE 6: Calculated Equilibrium Bond Lengths (Å) and Bond Angles (deg) for GdX_3, GdX_3·IG, and GdX_3·IG_2 (IG = Ne, Ar, Xe, and N_2) Systems[a]

		TZ2D/UHF				TZ2D/MP2			
	symmetry	R_{Gd-X}	Θ	R_{Gd-IG}	ΔE^b	R_{Gd-X}	Θ	R_{Gd-IG}	ΔE^b
GdF_3		2.059	120			2.048	118.5		
GdF_3·Ne	C_{3v}	2.060	119.8	2.935	−0.8 (−0.5)	2.050	119.1	2.734	−2.4 (−1.3)
GdF_3·Ne_2	D_{3h}	2.061	120	2.953	−1.5 (−1.0)	2.054	120	2.735	−4.8 (−2.3)
GdF_3·Ar	C_{3v}	2.060	119.3	3.298	−1.3 (−1.1)	2.051	118.1	3.030	−3.9 (−2.7)
GdF_3·Ar_2	D_{3h}	2.063	120	3.327	−2.3 (−1.8)	2.057	120	3.038	−7.1 (−4.7)
GdF_3·Xe	C_{3v}	2.061	118.7	3.635	−2.1 (−1.8)	2.051	117.5	3.388	−5.8 (−3.8)
GdF_3·Xe_2	D_{3h}	2.065	120	3.710	−3.2 (−2.6)	2.059	120	3.405	−10.2 (−6.1)
GdF_3·N_2	C_{3v}	2.064	119.4	2.815	−6.0 (−5.5)	2.056	119.4	2.663	−10.5 (−8.2)
GdF_3·$(N_2)_2$	D_{3h}	2.070	120	2.837	−11.1 (−10.2)	2.064	120	2.676	−20.4 (−16.3)
$GdCl_3$	D_{3h}	2.524	120			2.486	120		
$GdCl_3$·Ne	C_{3v}	2.525	119.8	2.911	−0.8 (−0.5)	2.487	119.5	2.689	−3.0 (−1.5)
$GdCl_3$·Ne_2	D_{3h}	2.528	120	2.943	−1.5 (−0.8)	2.490	120	2.703	−5.7 (−2.6)
$GdCl_3$·Ar	C_{3v}	2.528	119.4	3.225	−1.6 (−1.3)	2.489	119.1	2.963	−5.1 (−3.6)
$GdCl_3$·Ar_2	D_{3h}	2.532	120	3.302	−2.5 (−1.9)	2.495	120	2.990	−9.4 (−6.2)
$GdCl_3$·Xe	C_{3v}	2.530	118.9	3.563	−2.6 (−2.2)	2.490	118.7	3.303	−7.8 (−5.2)
$GdCl_3$·Xe_2	D_{3h}	2.536	120	3.671	−3.8 (−3.1)	2.499	120	3.346	−14.1 (−8.8)
$GdCl_3$·N_2	C_{3v}	2.533	119.5	2.754	−7.2 (−6.6)	2.494	119.9	2.589	−13.4 (−10.3)
$GdCl_3$·$(N_2)_2$	D_{3h}	2.543	120	2.784	−13.2 (−12.0)	2.502	120	2.619	−25.9 (−19.4)

[a] The Stabilization energies (kcal/mol) have been computed with respect to the isolated GdX_3 molecule and the isolated inert-gas unit. [b] Stabilization energies corrected for basis set superposition error are given in parentheses.

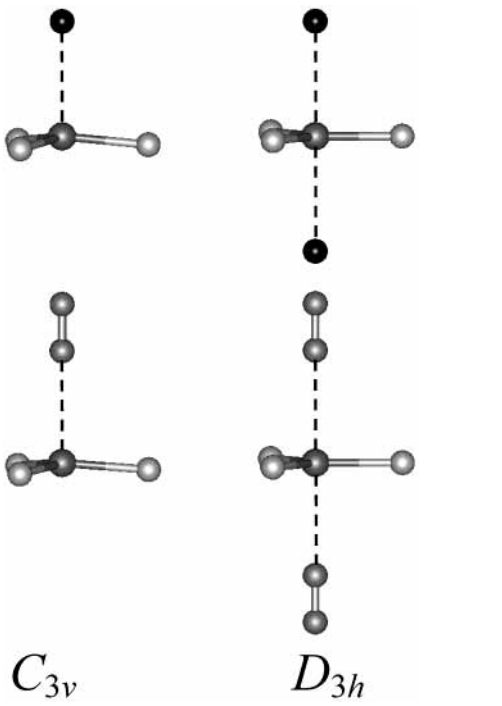

Figure 3. Molecular structures of GdF_3·Ne and GdF_3·N_2 (C_{3v} symmetry) complexes and GdF_3·Ne_2 and GdF_3·$(N_2)_2$ (D_{3h} symmetry) complexes.

not quenched by the coordination of a single inert-gas atom (or molecule) and the complexation of two species is the process that is energetically favored. Therefore, the GdX_3·IG_2 complex is a better model than the GdX_3·IG complex to simulate host−guest interactions between GdX_3 molecules and inert-gas matrices in real systems.

(4) There is a gradual increase of stabilization energy on passing from Ne to Ar to Xe and N_2 due to the enhanced polarizability. Mulliken charges on atoms for the $GdCl_3$·$(N_2)_2$ complex (Figure 4) suggest a strong ion−dipole interaction with an electron density accumulation on the nitrogen atom "bonded" to the gadolinium and a substantial positive charge on the nitrogen-end atom. These data also reveal a consistent electron density transfer from the $(N_2)_2$ framework to the $GdCl_3$

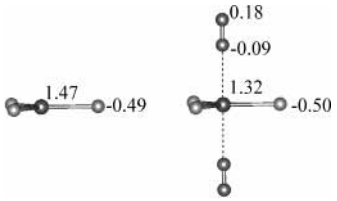

Figure 4. Atomic Mulliken charges for $GdCl_3$ and $GdCl_3$·$(N_2)_2$ complexes.

molecule. These electronic structure features lead to the formation of a weak Gd−N_2 bond (bond order is 0.19) and to a slight reduction of the N≡N triple bond (3.05→2.68).

(5) Because of the greater positive metal charge on the gadolinium atom in GdF_3 than in $GdCl_3$ derived from the Mulliken population, we would expect a greater complexation energy for GdF_3·IG_2. However, the reverse was found. Probably, this is due to greater steric nonbonding repulsive interactions between halogen pairs and inert-gas atoms (molecules) in GdF_3·IG_m complexes.

All the GdX_3·IG complexes adopt a pseudotetrahedral arrangement at the gadolinium atom with C_{3v} symmetry. The trigonal-planar structure of the isolated $GdCl_3$ species becomes pyramidal for all the $GdCl_3$·IG complexes with a small bond angle reduction (≤1.7°). The bond angle of the GdF_3 framework of GdF_3·IG complexes undergoes small changes. At the UHF level the bond angle always diminishes (planar → pyramidal). For GdF_3·Ar and GdF_3·Xe it decreases also at the MP2 level while it widens for GdF_3·Ne and GdF_3·N_2 complexes and geometries become closer to the trigonal planar.

The molecular geometry of GdX_3·IG_2 complexes is ubiquitously a trigonal bipyramid (D_{3h} symmetry), thus the symmetric coordination of two inert-gas molecules invariably leads to the planar GdX_3 framework. This finding, however, cannot allow us to conclude that GdX_3 molecules in matrices assume planar structures because of the simplicity of the adopted model. In any case, at present, this aspect does not seem to be fully settled experimentally.[5−7]

The R_{Gd-IG} contact diminishes substantially on passing from UHF to MP2 levels (∼0.25 Å), indicating an enhanced interaction in agreement with increased complexation energy discussed above (point 1). The R_{Gd-IG} contact of GdX_3·IG_2 is

TABLE 7: Harmonic Vibrational Frequencies (cm^{-1}) of GdX_3, GdX_3·IG, and GdX_3·IG_2 (IG = Ne, Ar, Xe, and N_2) Systems[a]

	TZ2D/UHF				MP2				experiment[4−6]			
	ν_1	ν_2	ν_3	ν_4	ν_1	ν_2	ν_3	ν_4	ν_1	ν_2	ν_3	ν_4
GdF_3	565.7	41.2	550.7	135.3	565.2	36.9	551.3	132.7	(583 ± 10)[b]		(552 ± 10)[b]	
GdF_3·Ne	564.5	47.8	549.4	135.4	561.9	35.1	548.9	132.1				
GdF_3·Ne_2	563.0	50.7	548.2	135.0	558.3	32.4	546.3	131.1	560.2	94	537.3	138
GdF_3·Ar	563.7	61.5	548.0	135.5	561.0	51.9	547.0	132.4				
GdF_3·Ar_2	560.0	57.5	545.4	134.5	553.6	50.8	541.8	130.2	544.7	100	519.2	133
GdF_3·Xe	562.1	68.9	546.0	135.4	559.5	52.0	544.7	132.3				
GdF_3·Xe_2	556.2	60.7	541.6	133.7	548.8	53.9	536.8	128.8				
GdF_3·N_2	559.1	62.1	544.1	134.0	554.7	44.8	542.4	130.5				
GdF_3·$(N_2)_2$	551.3	72.5	537.3	131.1	545.8	62.3	534.0	127.3	532	116 123	500	143
$GdCl_3$	323.6	42.5	339.9	77.1	331.6	24.2	353.2	74.6		35−85[c]	335[c]	77[c]
$GdCl_3$·Ne	322.8	47.5	338.8	77.2	331.2	37.1	352.0	74.8				
$GdCl_3$·Ne_2	321.3	52.1	337.3	77.3	329.3	47.5	350.5	75.3				
$GdCl_3$·Ar	321.4	51.3	336.8	77.2	329.8	43.7	350.0	74.8				
$GdCl_3$·Ar_2	318.7	58.9	334.6	76.9	325.4	59.7	346.5	75.1				
$GdCl_3$·Xe	320.0	59.9	334.8	77.0	328.3	42.8	348.0	74.8				
$GdCl_3$·Xe_2	315.0	59.5	330.8	76.1	321.7	59.0	342.6	73.9		53	318	82
$GdCl_3$·N_2	318.5	55.4	334.1	76.3	326.5	47.7	348.1	73.9				
$GdCl_3$·$(N_2)_2$	312.4	68.5	328.1	75.0	321.5	61.4	343.1	73.4				

[a] Only intramolecular GdX_3 frequencies are reported, see Figure 5. [b] Extrapolated from inert-gas matrix data. [c] Estimated from Figure 1 of ref 4b.

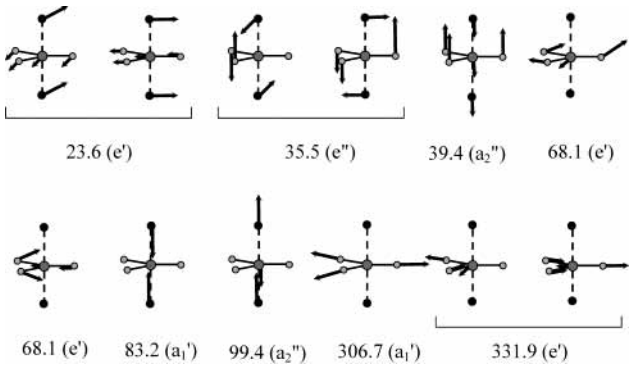

Figure 5. Schematic view of all normal modes for the $GdCl_3$·Ar_2 systems.

only slightly longer than that computed for the homologue GdX_3·IG complex in agreement with an almost double stabilization energy computed for GdX_3·IG_2 complexes (point 3). Analogously, R_{Gd-IG} contact in fluoride complexes is longer than in the corresponding chloride complexes (point 5).

The coordination of inert-gas atoms (or molecules) induces a significant increment of the Gd−X bond distances because of the IG→GdX_3 electron density transfer (Figure 4) that slightly destabilizes GdX_3 molecular orbitals, thus weakening Gd−X bonds. The lengthening follows the complexation energy, it increases on passing from the UHF to MP2 wave functions, grows along the series Ne < Ar < Xe < N_2, and for GdX_3·IG_2 complexes it is almost double that found for homologous GdX_3·IG complexes.

The GdX_3 molecules in the D_{3h} point group have four fundamental vibrations: the symmetric ν_1 (a_1') and asymmetric stretching ν_3 (e′) and the out-of-plane ν_2 (a_2'') and in-plane ν_4 (e′) bending. For GdX_3·IG_2 complexes (for simplicity we avoid discussion of GdX_3·$(N_2)_2$ systems) in the D_{3h} point group there are four additional vibrations having the following symmetry: e′, e″, a_1', and a_2''. Figure 5 displays schematically individual MP2 normal modes of the $GdCl_3$·Ar_2 complex (only dominant eigenvector contributions are represented). All of the ν_1, ν_2, ν_3, and ν_4 modes of isolated $GdCl_3$ have appropriate symmetry to interact with "new vibrations", thus they will be slightly shifted. The coupling is particularly strong for the large-amplitude ν_2 mode that undergoes a very large frequency shift. For other normal modes the coupling is small but not negligible and generally it leads to a frequency reduction. Because of the high symmetry of molecules and of weak coupling it is easy to separate internal vibrations of GdX_3 molecules and those involving inert-gas atoms (or molecules), thus in Table 7 only intramolecular GdX_3 frequencies are reported.

On comparing the ν_2 frequency mode of isolated GdX_3 molecules and those computed for GdX_3·IG_m complexes (Table 7), it is evident that interactions of GdX_3 molecules with the inert-gas matrices profoundly affect out-of-plane bending and the molecules become stiffer. For the $GdCl_3$ the ν_2 frequency mode increases substantially on passing from the isolated molecule to inert-gas complexes and the increment is roughly proportional to the interaction energy. Thus, the ν_2 frequency grows along the series Ne < Ar ≈ Xe < N_2 and on passing from $GdCl_3$·IG to $GdCl_3$·IG_2. In regard to the GdF_3 molecule, because of its greater tendency to adopt a pyramidal structure, the ν_2 frequency shift is not as regular as interaction energy augments. In particular, the ν_2 frequency increases monotonically on going to GdF_3·N_2 and to GdF_3·$(N_2)_2$ complexes at both UHF and MP2 levels. It grows on going from GdF_3 to GdF_3·Ar or to GdF_3·Xe while it changes slightly as another atom of Ar or Xe is coordinated. For neon complexes the ν_2 frequency increases monotonically on going to GdF_3·Ne and to GdF_3·Ne_2 at the UHF level while it diminishes monotonically on going to GdF_3·Ne and to GdF_3·Ne_2 at the MP2 level.

The ν_4 scissors-type bending frequency is almost insensitive to the coordination of one or two noble gas atoms (differences are less than 1.6 cm^{-1}) and only a small reduction, 2.5, 3.9, 2.2, and 5.4 cm^{-1}, is observed for GdF_3·Ar_2, GdF_3·Xe_2, GdF_3·N_2, and GdF_3·$(N_2)_2$, respectively.

Even the stiff stretching modes are affected by the host matrix (Table 7), thus a consistent lowering of both ν_1 and ν_3 frequency modes is noticed on passing from isolated molecules GdX_3 to inert-gas complexes GdX_3·IG_m in agreement with the R_{Gd-X} bond weakening discussed above. The reduction is roughly proportional to the interaction energy. Thus the frequency shift increases (i) on passing from the UHF to the MP2 wave function, (ii) along the series Ne < Ar < Xe < N_2, and (iii) on passing from GdX_3·IG to GdX_3·IG_2.

Measured IR frequencies[5] for $GdCl_3$ molecules trapped in the xenon matrix at 20−30 K are reported in Table 7 together with $GdCl_3$ gas-phase experimental (1350 K) data[4b] and present theoretical results. On going from the gas-phase to the xenon matrix the ν_3 frequency undergoes a consistent reduction (∼15 cm^{-1}) as qualitatively predicted by calculations for $GdCl_3 \cdot Xe_2$ model complexes (10.6 cm^{-1}). Experimental gas-phase/matrix comparison for ν_2 and ν_4 is hampered by the huge indetermination in gas-phase estimations of fundamental frequencies. On the other hand there is good agreement on ν_2 and ν_4 frequencies measured in the xenon matrix and those computed for the $GdCl_3 \cdot Xe_2$ model at both UHF and MP2 levels. These data demonstrate that unfavorable comparison of frequencies observed in the IR spectra of inert matrix-isolated LnX_3 molecules and gas-phase ab initio derived frequencies[17] is not due to a shortcoming of the theoretical approach but rather to the absence of any matrix effect correction.

Unfortunately, no experimental data have been reported for the gas-phase GdF_3 molecule. However, the ν_1 and ν_3 gas-phase vibrational frequencies have been estimated from data obtained through matrix isolation techniques at ∼15 K (Table 7) by the following empirical approximation[6]

$$\nu_{gas} \approx \nu_{Ne} + (0.8 \pm 0.4)(\nu_{Ne} - \nu_{Ar}) \qquad (12)$$

For the ν_2 and ν_4 bending fundamentals simple empirical relations cannot be derived because the direction of matrix shifts depend on the nature of the vibrational mode. Thus, the observed shift of ν_2 sometimes is in the opposite direction to that measured for the ν_4 mode. In addition, because molecules can occupy various sites in the embedded matrix, the molecular shape might be slightly different because of the very flat potential energy curve for out-of-plane distortion and the very weak ν_2 mode absorption band can appear as a doublet (GdF_3 in the nitrogen matrix, Table 7).[6,7]

Present data are in agreement with main spectra features experimentally observed.[6,7] Thus, different $GdF_3 \cdot IG_m$ model complexes yielded successively smaller ν_1 and ν_3 frequencies for matrices with increased attractive host−guest interaction. However, computed shifts (∼6, ∼10, and ∼18 cm^{-1} for Ne, Ar, and N_2, respectively) are less than those estimated experimentally (∼19, ∼35, and ∼51 cm^{-1} for Ne, Ar, and N_2, respectively) because of the simplified model adopted in computation. Also for the ν_2 and ν_4 bending frequencies there is a good qualitative agreement between computed and observed frequency shift. Indeed, computed ν_2 frequency increases substantially as GdF_3- - -IG_m interaction grows, as experimentally observed, and computed absolute values are closer to those measured. Experimental ν_4 frequency is slightly affected by matrix changes and frequency shift is not regular. It lowers slightly from Ne to Ar matrices and it increases slightly on passing to the N_2 matrix. Computed ν_4 frequencies show a small reduction on increasing interaction energy in agreement with small shifts in experimental observations. Also the experimental ν_4 frequency reduction on passing from Ne to Ar matrices is well reproduced by proposed models while our simplified model does not account for the frequency increase obtained in the N_2 matrix.

Conclusions

The present theoretical analysis provides a quantitative and comprehensive study and a detailed theoretical/experimental comparison on molecular properties of gadolinium trihalides explicitly including temperature, anharmonicity, and inert-gas matrix effects. Striking and instructive differences are detected with respect to molecular properties derived from potential energy minimum, i.e., equilibrium structures and harmonic frequencies of isolated GdX_3 species. Due to the soft angle deformation motion the thermal average structures in the examined molecules are substantially more pyramidal than the equilibrium structures. For $GdCl_3$ the average structure symmetry is lower than the equilibrium arrangement, in excellent agreement with experiments. Calculations performed on simple $GdX_3 \cdot IG$ and $GdX_3 \cdot IG_2$ complexes to model inert-gas interactions show that equilibrium structures are strongly influenced by the embedding medium. Therefore, structures obtained from gas-phase measurements might considerably deviate from those derived in matrix-isolated techniques.

Computed anharmonic vibrational frequencies for an isolated $GdCl_3$ molecule allow a rational and exhaustive interpretation of the high-temperature gas-phase IR spectrum. On the other hand, computed frequencies for $GdX_3 \cdot IG$ and $GdX_3 \cdot IG_2$ complexes differ from those obtained for the gas phase especially for the out-of-plane mode. The excellent agreement between frequencies experimentally measured in inert-gas matrices and those computed for $GdX_3 \cdot IG_2$ demonstrates that spectroscopy accuracy can only be reached by including matrix effects.

References and Notes

(1) Hargittai, M. *Chem. Rev.* **2000**, *100*, 2233.

(2) (a) Hargittai, M. *J. Phys. Chem. A* **1999**, *103*, 7552. (b) Molnar, J.; Marsden, C. J.; Hargittai, M. *J. Phys. Chem.* **1995**, *99*, 9062.

(3) Beattie, I. R. *Angew. Chem., Int. Ed.* **1999**, *38*, 3294.

(4) (a) Kovacs, A.; Konings, R. J. M.; Booij, A. S. *Chem. Phys. Lett.* **1997**, *268*, 207. (b) Kovacs, A.; Konings, R. J. M.; Booij, A. S. *Vib. Spectrosc.* **1995**, *10*, 65. (c) Selivanov, G. K.; Sekachev, Y. N.; Mal'tsev, A. A. *Russ. J. Phys. Chem.* **1973**, *47*, 1239.

(5) Perov, P. A.; Nedyak, S. V.; Mal'tsev, A. A. *Vestn. Mosk. Univ. Khim.* **1975**, *16*, 281.

(6) (a) Hauge, R. H.; Hastie, J. W.; Margrave, J. L. *J. Less-Common Met.* **1971**, *23*, 359. (b) Hauge, R. H.; Hastie, J. W.; Margrave, J. L. *J. Less-Common Met.* **1975**, *39*, 309.

(7) (a) Wesley, R. D.; DeKock, C. W. *J. Chem. Phys.* **1971**, *55*, 3866. (b) Leisiecki, M.; Nibler, J. W.; DeKock, C. W. *J. Chem. Phys.* **1972**, *57*, 1352.

(8) Asovich, V. S.; Kornilov, V. V.; Maksimov, B. N. *Zh. Prikl. Khim.* **1994**, *67*, 107.

(9) Caird, J. A.; Carnal, W. T.; Hessler, J. P.; Williams, C. W. *J. Chem. Phys.* **1981**, *74*, 798.

(10) McPhall, D. S.; Hocking, M. G.; Jeffes, J. H. E. *J. Mater. Sci.* **1985**, *20*, 1457.

(11) Hake, D.; Urland, W. *Z. Anorg. Allg. Chem.* **1992**, *613*, 45.

(12) Murase, K.; Ozaki, T.; Machida, K.; Adachi, G. *J. Alloys Compd.* **1996**, *233*, 96.

(13) Murase, K.; Machida, K.; Adachi, G. *J. Alloys Compd.* **1995**, *217*, 218.

(14) Réffy, B.; Marsden, C. J.; Hargittai, M. *J. Phys. Chem. A* **2003**, *107*, 1840.

(15) (a) Girichev, N. I.; Zakharov, A. V.; Shlykov, S. A.; Girichev, G. V. *J. Chem. Soc., Dalton Trans.* **2000**, 3401. (b) Zasorin, E. Z.; Ivanov, A. A.; Ermolaeva, L. I.; Spiridonov, V. P. *Zh. Fiz. Khim.* **1989**, *63*, 669.

(16) Dolg, M.; Stoll, H.; Preuss, H. *J. Mol. Struct. (THEOCHEM)* **1991**, *235*, 67.

(17) (a) Di Bella, S.; Lanza, G.; Fragalà, I. L. *Chem. Phys. Lett.* **1993**, *214*, 598. (b) Lanza, G.; Fragalà, I. L. *Chem. Phys. Lett.* **1996**, *255*, 341. (c) Lanza, G.; Fragalà, I. L. *J. Phys. Chem. A* **1998**, *41*, 7995.

(18) Cundari, T. R.; Sommerer, S. O.; Strohecker, L. A.; Tippett, L. *J. Chem. Phys.* **1995**, *103*, 7085.

(19) (a) Adamo, C.; Maldivi, P. *J. Phys. Chem. A* **1998**, *102*, 6812. (b) Adamo, C.; Barone, V. *J. Comput. Chem.* **2000**, *21*, 1153.

(20) (a) Joubert, L.; Picard, G.; Legendre, J.-J. *J. Alloys Compd.* **1998**, *275−277*, 934. (b) Joubert, L.; Picard, G.; Legendre, J.-J. *Inorg. Chem.* **1998**, *37*, 1984.

(21) Solomonik, V. G.; Marochko, O. Y. *J. Struct. Chem.* (*Engl. Transl.*) **2000**, *41*, 725.

(22) Tsuchiya, T.; Taketsugu, T.; Nakano, H.; Hirao, K. *J. Mol. Struct. (THEOCHEM)* **1999**, *461−462*, 203.

(23) Jansik, B.; Sanchez de Meras, A. M. J.; Schimmelpfenning, B.; Ågren, H. *J. Chem. Soc., Dalton Trans.* **2002**, 4603.

(24) Lanza, G.; Minichino, C. *ChemPhysChem* **2004**, *5*, 120.
(25) (a) Cundari, T. R.; Stevens, W. J. *J. Chem. Phys.* **1993**, *98*, 5555. (b) Stevens, W. J.; Krauss, M.; Basch, H.; Jasien, P. G. *Can. J. Chem.* **1992**, *70*, 612.
(26) Dunning, T. H., Jr. *J. Chem. Phys.* **1971**, *55*, 716.
(27) McLean, A. D.; Chandler, G. S. *J. Chem. Phys.* **1980**, *72*, 5639.
(28) Schmidt, M. W.; Baldridge, K. K.; Boatz, J. A.; Elbert, S. T.; Gordon, M. S.; Jensen, J. H.; Koseki, S.; Matsunaga, N.; Nguyen, K. A.; Su, S. J.; Windus, T. L.; Dupuis, M.; Montgomery, J. A. *J. Comput. Chem.* **1993**, *14*, 1347.
(29) (a) Cao, X.; Dolg, M. *J. Mol. Struct.* (*THEOCHEM*) **2002**, *581*, 139. (b) Cao, X.; Dolg, M. *J. Chem. Phys.* **2001**, *115*, 7348.
(30) Frisch, M. J.; Trucks, G. W.; Schlegel, H. B.; Scuseria, G. E.; Robb, M. A.; Cheeseman, J. R. V.; Zakrzewski, G.; Montgomery, J. A., Jr.; Stratmann, R. E.; Burant, J. C.; Dapprich, S.; Millam, J. M.; Daniels, A. D.; Kudin, K. N.; Strain, M. C.; Farkas, O.; Tomasi, J.; Barone, V.; Cossi, M.; Cammi, R.; Mennucci, B.; Pomelli, C.; Adamo, C.; Clifford, S.; Ochterski, J.; Petersson, G. A.; Ayala, P. Y.; Cui, Q.; Morokuma, K.; Malick, D. K.; Rabuck, A. D.; Raghavachari, K.; Foresman, J. B.; Cioslowski, J.; Ortiz, J. V.; Stefanov, B. B.; Liu, G.; Liashenko, A.; Piskorz, P.; Komaromi, I.; Gomperts, R.; Martin, R. L.; Fox, D. J.; Keith, T.; Al-Laham, M. A.; Peng, C. Y.; Nanayakkara, A.; Gonzalez, C.; Challacombe, M.; Gill, P. M. W.; Johnson, B.; Chen, W.; Wong, M. W.; Andres, J. L.; Gonzalez, C.; Head-Gordon, M.; Replogle, E. S.; Pople, J. A. *Gaussian 98*, Revision A.6; Gaussian, Inc.: Pittsburgh, PA, 1998.
(31) (a) Bowman, J. M. *Acc. Chem. Res.* **1986**, *19*, 202. (b) Chaban, G. M.; Jung, J. O.; Gerber, R. B. *J. Chem. Phys.* **1999**, *111*, 1823. (c) Chaban, G. M.; Jung, J. O.; Gerber, R. B. *J. Phys. Chem. A* **2000**, *104*, 2772.
(32) Leonard, C.; Carter, S.; Handy, N. C. *Chem. Phys. Lett.* **2003**, *370*, 360.
(33) (a) Barone, V.; Grand, A.; Minichino, C.; Subra, R. *J. Chem. Phys.* **1993**, *99*, 6787. (b) Minichino, C.; Barone, V. *J. Chem. Phys.* **1994**, *100*, 3717.
(34) Daasch, W. R.; Werden, S.; Feller, D.; Davidson, E. R. *J. Mol. Struct.* (*THEOCHEM*) **1983**, *103*, 177.
(35) De Boor, C. *A practical guide to spline*; Springer-Verlag: New York, 1978.
(36) Cremaschi, P. *Mol. Phys.* **1980**, *40*, 401.
(37) (a) Raghavachari, K.; Anderson, J. B. *J. Phys. Chem.* **1996**, *100*, 12960. (b) Head-Gordon, M. *J. Phys. Chem.* **1996**, *100*, 13213. (c) Ziegler, T. *Chem. Rev.* **1991**, *91*, 651. (d) Jensen, F. *Introduction to Modern Computational Chemistry*; Wiley: New York, 1999.
(38) Kaupp, M.; Schleyer; P. v. R.; Stoll, H. *J. Phys. Chem.* **1992**, *96*, 9801.
(39) Bihary, Z.; Chaban, G. M.; Gerber, R. B. *J. Chem. Phys.* **2002**, *116*, 5521.
(40) Wells, A. F. *Structural Inorganic Chemistry*; Clarendon Press: Oxford, UK, 1975; p 356.
(41) Malandrino, G.; Incontro, O.; Castelli, F.; Fragalà, I. L.; Benelli, C. *Chem. Mater.* **1996**, *8*, 1292.